

SUPERHEAVY TOROIDAL NUCLEI IN THE SKYRME ENERGY FUNCTIONAL FRAMEWORK*

A. KOSIOR¹, A. STASZCZAK¹ AND CHEUK-YIN WONG²

¹Institute of Physics, Maria Curie-Skłodowska University, Lublin, Poland

²Physics Division, Oak Ridge National Laboratory, Oak Ridge, TN USA

Using the Hartree-Fock-Bogoliubov (HFB) self-consistent mean-field theory with the SkM* Skyrme energy-density functional, we study nuclear structure properties of even-even superheavy nuclei (SHN) of $Z = 120$ isotopes and $N = 184$ isotones. The shape of the nucleus along the lowest energy curve as a function of the quadrupole moment Q_{20} makes a sudden transition from the oblate spheroids (biconcave discs) to the toroidal shapes, in the region of large oblate quadrupole moments.

PACS numbers: 21.60.-n, 21.60.Jz, 25.85.Ca, 27.90.+b

1. Introduction

Since the time when Wheeler coined the name *superheavy nuclei* (SHN) in 1955 [1], our knowledge of the “very heavy nuclei” has become more extensive and systematic. During the last 60 years the heaviest known nucleus limit has been extended from ${}_{101}^{256}\text{Md}$ (1955) [2] to ${}_{118}^{294}\text{Og}$ (2006) [3], and the properties of SHN have been studied mostly in the region of prolate deformations. In this region, the energy surfaces of SHN reveal two paths to fission: a reflection-symmetric path corresponding to elongated fission fragments (sEF) and the reflection-asymmetric path with elongated fission fragments (aEF), which bifurcates from the sEF path after the first barrier, see e.g. Ref. [4]. There are also predictions on the ground state deformations, fission barrier heights, and spontaneous-fission and α -decay half-lives of SHN; for a recent review, see for example Refs. [5, 6].

Theoretically, the properties of SHN have been studied much less in the oblate region than in the prolate region, with a few exceptions, such as the study on super-deformed-oblate SHN at quadrupole moment $Q_{20} = -60$

* Presented at the XXIII Nuclear Physics Workshop “Marie and Pierre Curie”, Kazimierz Dolny, Poland, 27th Sept. - 2nd Oct., 2016

to -55 b [7, 5]. Within the self-consistent constraint Skyrme-Hartree-Fock+BCS model, we found equilibrium toroidal nuclear density distributions at oblate deformation $Q_{20} \leq -200$ b for the hypothetical SHN $^{316}122$, $^{340}130$, $^{352}134$, and $^{364}138$ [8].

It is interesting to note that it was also Wheeler who suggested long ago that under appropriate conditions the nuclear fluid may assume a toroidal shape [9]. In 1970's the idea of a toroidal nucleus was examined in the framework of the liquid drop model and shell corrections [10, 11].

This contribution is devoted to a systematic investigation on the chain of even-even $Z = 120$ isotopes and $N = 184$ isotones within the self-consistent constraint Skyrme-Hartree-Fock-Bogoliubov (Skyrme-HFB) mean-field theory at the region of large oblate deformations.

2. Model and results

The constrained Skyrme-HFB approach is equivalent to the minimization of the Skyrme energy density functional $E^{tot}[\bar{\rho}]$ with respect to the densities and currents under appropriate constraints [12]. Using the method of Lagrange multipliers we solve an equality-constrained problem (ECP):

$$\left\{ \begin{array}{l} \min_{\bar{\rho}} E^{tot}[\bar{\rho}] \\ \text{subject to: } \langle \hat{N}_q \rangle = N_q, \quad (q = p, n), \\ \langle \hat{Q}_{\lambda\mu} \rangle = Q_{\lambda\mu}, \end{array} \right. \quad (1)$$

where the constraints are defined by the average values $N_{p,n}$ of the proton and neutron particle-number operators $\hat{N}_{p,n}$ and by the constrained values $Q_{\lambda\mu}$ of the mass-multiple-moment operators $\hat{Q}_{\lambda\mu}$.

The above ECP equations were solved using an augmented Lagrangian method [13] with the symmetry-unrestricted code HFODD [14]. In the particle-hole channel the Skyrme SkM* [15] force was applied and a density-dependent mixed pairing interaction [4] in the particle-particle channel was used. The code HFODD uses the basis expansion method utilizing a three-dimensional Cartesian deformed harmonic oscillator basis. In the present study, we used a basis which consists of states having not more than $N = 26$ quanta in the Cartesian directions, and not more than 1140 states.

As an example, the total HFB energy of SH nucleus $^{304}120_{184}$ as a function of the quadrupole moment Q_{20} is shown in Fig. 1. In addition to a spherical ground state minimum, one can see two paths leading to fission on the prolate side: a reflection-symmetric path with the elongated fission fragments (sEF) (open circles) and a reflection-asymmetric path with the elongated fission fragments (aEF) (dashed line). On the oblate side, the self-consistent nuclear density under the Q_{20} constraint changes from an

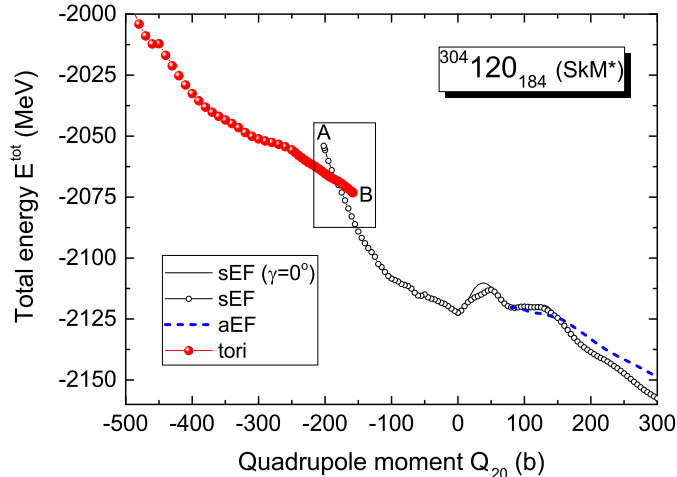


Fig. 1. (Color online.) Total HFB energy of $^{304}_{120}_{184}$ as a function of the quadrupole moment. The open circle symbols and dashed (blue) line show the symmetric (sEF) and asymmetric (aEF) elongated fission pathways, respectively. The axially symmetric sEF ($\gamma = 0^\circ$) fission pathway is marked by a solid thin line. The nuclear matter density distributions with toroidal shapes appear in the region of large oblate deformation $Q_{20} \leq -158$ b as (red) solid circles.

oblate spheroidal to a biconcave disc shape, as the magnitude of oblate Q_{20} increases. When the oblate Q_{20} magnitude exceeds 158 b, there emerges an additional self-consistent toroidal nuclear density solution.

An enlarged view of the transition from the biconcave disc to the toroidal shape of Fig. 1 is shown in Fig. 2(a), where our Skyrme-HFB calculations give the biconcave disc solutions ending at the point **A** (at $Q_{20}(\mathbf{A}) = -202$ b), and another toroidal solutions starting at the point **B** (at $Q_{20}(\mathbf{B}) = -158$ b). The nuclear density distributions of $^{304}_{120}_{184}$ calculated at **A** and **B** are depicted in Fig. 2(b), which indicates that the nuclear density at the toroidal geometrical center is very small at the starting point **B** of the toroidal sequence, but remains to be about $0.08/\text{fm}^3$ at point **A** of the biconcave disc sequence.

In the region of quadrupole moment between $Q_{20}(\mathbf{A})$ and $Q_{20}(\mathbf{B})$, both biconcave disc and toroidal solutions coexist for $^{304}_{120}_{184}$. It is of interest to examine the single-particle states of these two types of solutions in this oblate deformation region. The proton single-particle levels of $^{304}_{120}_{184}$ close to the Fermi energy as a function of Q_{20} between $Q_{20}(\mathbf{A})$ and $Q_{20}(\mathbf{B})$ for the biconcave disc and toroidal sequences are shown in the upper and lower panels of Fig. 3, respectively. Levels with positive parity are drawn

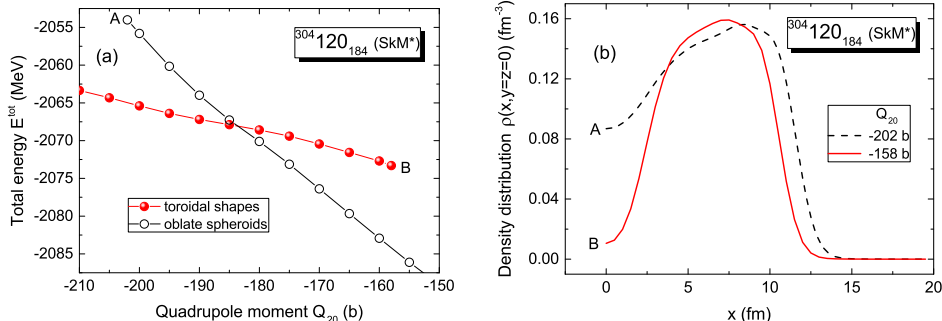


Fig. 2. (Color online.) Left panel (a), an enlarged view of Fig. 1, the total HFB energy of $^{304}_{120}_{184}$ as a function of the quadrupole moment between points **A**-**B**, where a shape transition from biconcave discs to toroidal shapes takes place. Right panel (b), the nuclear density distribution at $Q_{20}(\mathbf{A}) = -202$ b (biconcave disc) and $Q_{20}(\mathbf{B}) = -158$ b (torus).

as solid curves, while those with negative parity are drawn as dashed curves. Each single-particle state is labeled by the Nilsson quantum numbers $[N, n_z, \Lambda]\Omega$ of the dominant component. Each level is doubly degenerate. The circled numbers denote the occupation numbers. For the sake of comparison, Fig. 4 gives the neutron single-particle levels close to the Fermi energy for the biconcave disc solution in the upper panel and the toroidal solution in the lower panel.

Even though Figs. 3 and 4 pertain to the self-consistent single-particle states for $^{304}_{120}$, we expect that the mean-field potential depends mostly on nuclear density shape and the quadrupole moment, and varies only slightly as a function of the atomic number and the neutrons number. The single-particle state diagrams in Figs. 3 and 4 can be approximately applied to an extended region around $^{304}_{120}_{184}$.

We infer from Figs. 3 and 4 that the densities of proton and neutron single-particles states are far from being uniform. There are regions of sparse density of single-particle states which can be identified as single-particle “shells” associated with enhanced stability [16]. It will be of future interest to exploit the property of the extra stability of SHN for which the toroidal proton and neutron shells are located at the same deformation. The shell effects play an even more significant role when the bulk properties of the system lead to a nearly flat bulk energy as a function of the deformation, such as would be expected for systems with $Z \geq 122$ [8]. The complexity of the single-particle state energy level diagram indicates that the location of the neutron and proton shells needs to be examined on a case-by-case basis.

Fig. 5(a) gives the Skyrme-HFB energies as a function of the quadrupole

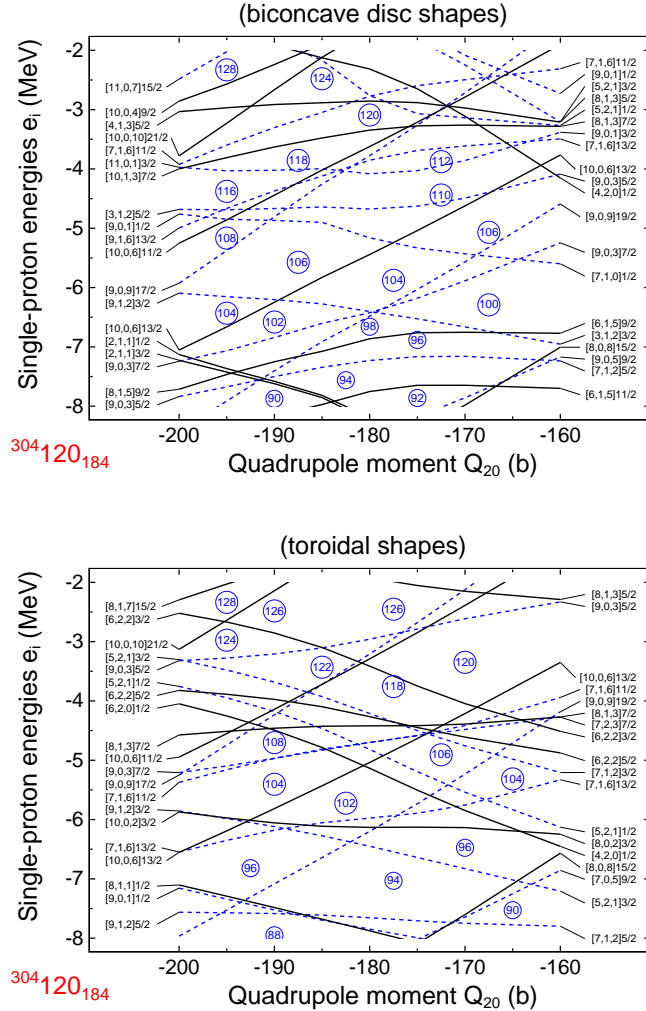


Fig. 3. (Color online.) Proton single-particle levels of $^{304}_{120}\text{184}$ as a function of the quadrupole moment. The levels with positive parity are drawn with solid lines, while those with negative parity are drawn with (blue) dashed lines. The upper panel is for a biconcave disc shape and the lower panel for a toroidal shape.

moment of even-even $Z = 120$ isotopes with the number of neutrons from 166 to 190, in the region of the shape transition from the biconcave disc shape to the toroidal shape. The toroidal and biconcave disc total energies decreases as a function of increasing Q_{20} and do not possess an energy minimum. The slope of the toroidal energy as a function of Q_{20} appears to be nearly independent of the neutron number, for $Z = 120$ isotopes. The

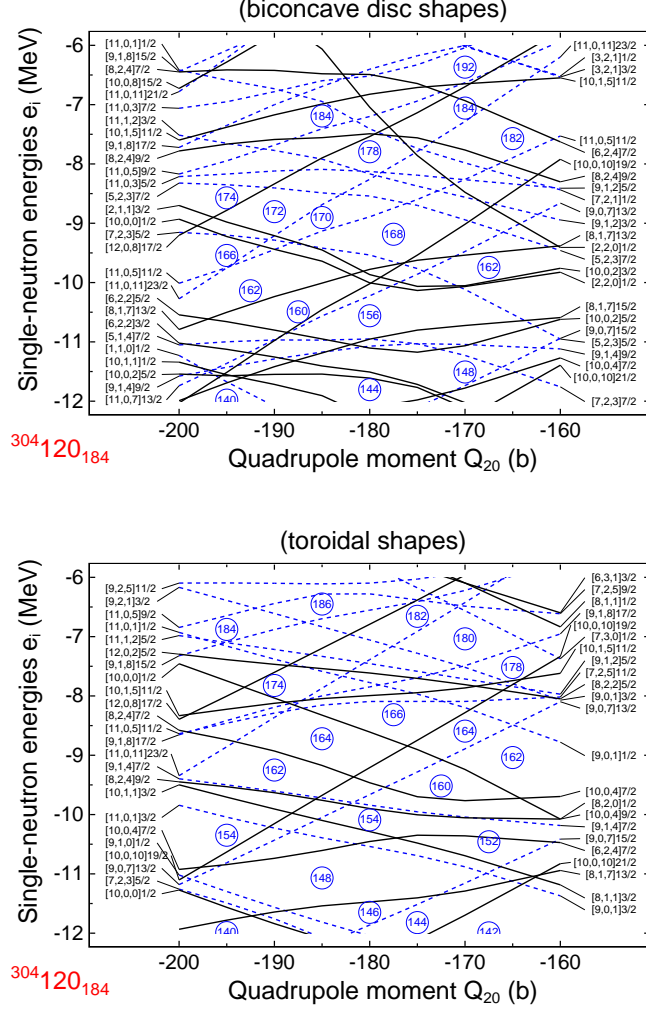


Fig. 4. (Color online.) The same as in Fig. 3, but for the neutron single-particle levels.

biconcave disc energy curve and the toroidal energy curve cross each other at an energy crossing point, whose location moves to a more negative Q_{20} value as the neutron number increases. Along the lowest energy curve as a function of Q_{20} in Fig. 5(a), there is a sudden shape transition from the biconcave disc shape to the toroidal shape at the energy crossing point. The first solution with the toroidal shape takes place at $Q_{20} = -150$ b for $N = 166$, and at $Q_{20} = -160$ b for $N = 190$.

Similar results, but for the even-even $N = 184$ isotones with the number

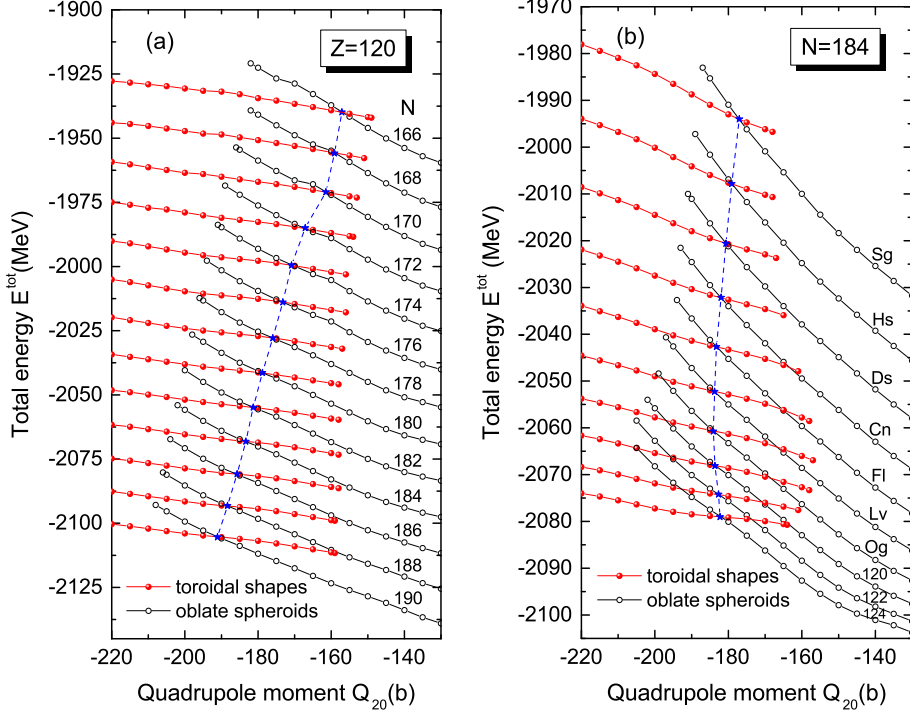


Fig. 5. (Color online.) Shape transitions from the biconcave disk shapes to the toroidal shapes for the even-even isotopes $Z = 120$ in panel (a), and for the even-even isotones $N = 184$ in panel (b). The points of energy crossing of the oblate spheroids and toroidal shapes solutions are connected by a (blue) dashed line.

of protons from 106 to 124 are shown in Fig. 5(b). For those isotones, one observes that as the proton number increases, the magnitude of the Coulomb repulsion increases, and the magnitude of the slope of the toroidal energy curve becomes smaller. The toroidal energy curve for $Z = 124$ is nearly but not completely flat. Further increase in the proton number may render a toroidal energy equilibrium at a greater oblate deformation. The energy crossing points of the biconcave disk and toroidal energy curves occur at $Q_{20} \approx -180$ b for all atomic numbers in Fig. 5(b).

3. Conclusions and Discussions

The Coulomb repulsion from a large number of protons in a SH nucleus has a tendency to push the nuclear matter outward, making it easier to assume a toroidal shape. We examine here SHN in the region of $Z = 120$ isotopes and $N = 184$ isotones. We find that as the magnitude of the

oblate Q_{20} increases along the lowest energy curve, there is a sudden shape transition from a biconcave disc to a torus. For $Z = 120$ isotopes with $166 \leq N \leq 190$ and for $N = 184$ isotones with $106 \leq Z \leq 124$, the total energy curves lie on a slope, indicating that these nuclei in a toroidal shape are unstable against returning to the shape of a sphere-like geometry.

Our examination of the single-particle states in this region reveal that the density of single-particle levels is far from being uniform and single-particle shells are present at various toroidal deformations. Because the energy curve as a function Q_{20} becomes flatter with increasing Z , one expects that by increasing the atomic number beyond $Z \geq 122$ with possible appropriate toroidal shells, some toroidal figures of equilibrium may become possible. Future search for toroidal nuclei may focus attention in this superheavy region in conjunction with possible nuclear shell effects.

The presence of a large angular momentum will facilitate the formation of a toroidal nucleus. In this regard, it will be useful to examine SHN with non-collective rotations whose spin along the symmetry axis arises from particle-hole excitations [17]. Previous investigation reveal a region of toroidal high-spin isomers in the light mass region [18, 19, 20, 21, 22, 23]. A recent investigation shows that $^{304}_{120}184$ with $I = I_z = 81$ and $208\hbar$ may be toroidal high-spin isomers [24].

The research was supported in part by the Division of Nuclear Physics, U.S. Department of Energy under Contract DE-AC05-00OR22725 and the National Science Center, Poland, project no 2016/21/B/ST2/01227.

REFERENCES

- [1] J. A. Wheeler, *Proc. Intern. Conf. on the Peaceful Uses of Atomic Energy, Geneva 1955, vol.2*, (United Nations New York 1956) p. 155.
- [2] A. Ghiorso, B. G. Harvey, G. R. Choppin, S. G. Thompson, and G. T. Seaborg, *Phys. Rev.* **98**, 1518 (1955).
- [3] Y. T. Oganessian *et al.*, *Phys. Rev. C* **74**, 044602 (2006).
- [4] A. Staszczak, A. Baran and W. Nazarewicz, *Phys. Rev. C* **87**, 024320 (2013).
- [5] P.-H. Heenen, J. Skalski, A. Staszczak, and D. Vretenar, *Nucl. Phys. A* **944**, 415 (2015).
- [6] A. Baran, M. Kowal, P.-G. Reinhard, L. M. Robledo, A. Staszczak, and M. Warda, *Nucl. Phys. A.* **944**, 442 (2015).
- [7] P. Jachimowicz, M. Kowal and J. Skalski, *Phys. Rev. C* **83**, 054302 (2011).
- [8] A. Staszczak and C. Y. Wong, *Acta Phys. Pol. B* **40**, 753 (2008).
- [9] See a reference to J. A. Wheeler's toroidal nucleus in G. Gamow, *Biography of Physics*, (New York: Harper & Brothers Publishers, 1961) pp. 297.
- [10] C. Y. Wong, *Ann. Phys.* **77**, 279 (1973).

- [11] C. Y. Wong, *Phys. Rev. C* **17**, 331 (1978).
- [12] E. Perlinska, S. G. Rohozinski, J. Dobaczewski, and W. Nazarewicz, *Phys. Rev. C* **69**, 014316 (2004).
- [13] A. Staszczak, M. Stoitsov, A. Baran, and W. Nazarewicz, *Eur. J. Phys. A* **46**, 85 (2010).
- [14] N. Schunck, J. Dobaczewski, J. McDonnell, W. Satuła, J. A. Sheikh, A. Staszczak, M. Stoitsov, and P. Toivanen, *Comput. Phys. Commun.* **183**, 166 (2012).
- [15] J. Bartel, P. Quentin, M. Brack, C. Guet, and H. B. Håkansson, *Nucl. Phys. A* **386**, 79 (1982).
- [16] M. Brack, J. Damgaard, A. S. Jensen, H. C. Pauli, V. M. Strutinsky, and C. Y. Wong, *Rev. Mod. Phys.* **44**, 320 (1972).
- [17] A. Bohr and B. R. Mottelson, *Nucl. Phys. A* **354**, 303c (1981).
- [18] T. Ichikawa, J. A. Maruhn, N. Itagaki, K. Matsuyanagi, P-G. Reinhard, and S. Ohkubo, *Phys. Rev. Lett.* **109**, 232503 (2012).
- [19] T. Ichikawa, K. Matsuyanagi, J. A. Maruhn, and N. Itagaki, *Phys. Rev. C* **89**, 011305(R) (2014).
- [20] A. Staszczak and C. Y. Wong, *Phys. Lett. B* **738**, 401 (2014).
- [21] A. Staszczak and C. Y. Wong, *Acta Phys. Pol. B* **46**, 675 (2015), arXiv:1504.07646.
- [22] A. Staszczak and C. Y. Wong, *Phys. Scripta* **90**, 114006 (2015), arXiv:1412.0050.
- [23] A. Staszczak and C. Y. Wong, *EPJ Web of Conferences* **117**, 04008 (2016), arXiv:1510.04610.
- [24] A. Staszczak, C. Y. Wong, and A. Kosior, (to be published).